Journal of Materials Chemistry

Cite this: *J. Mater. Chem.*, 2012, **22**, 1094

www.rsc.org/materials

PAPER

Nano-silicon composites using poly(3,4-ethylenedioxythiophene):poly (styrenesulfonate) as elastic polymer matrix and carbon source for lithium-ion battery anode

Lu Yue,[ab] Suqing Wang,[a] Xinyue Zhao[a] and Lingzhi Zhang*[a]

Received 14th September 2011, Accepted 14th October 2011
DOI: 10.1039/c1jm14568a

Nano-silicon composites, Si/poly(3,4-ethylenedioxythiophene):poly(styrenesulfonate) (PEDOT:PSS) and Si/C, were prepared by an *in situ* chemical polymerization of 3,4-ethylenedioxythiophene (EDOT) with nano-Si particles in a PSS aqueous solution and subsequent carbonization of Si/PEDOT:PSS, respectively. The nano-Si particles were embedded in a shapeless PEDOT:PSS matrix and amorphous carbon in the corresponding composite. Energy dispersive spectroscopy (EDS) and X-ray photoelectron spectroscopy (XPS) measurements revealed that 2.66 wt% of the element sulfur was doped in the carbon matrix for Si/C composite. Both the Si/PEDOT:PSS and Si/C composite electrodes exhibited higher initial coulombic efficiency and better cycling performance than the bare nano-Si anode. The Si/C composite showed the best electrochemical performance, retaining a specific capacity of 768 mA h g^{-1} and a Coloumbic efficiency of 99.2% after 80 cycles, with a very small initial capacity loss of 2.80% and a capacity fade of 0.48% per cycle.

1. Introduction

Silicon has attracted great attention as an anode material in rechargeable lithium-ion batteries because of its high theoretical specific capacity (*ca.* 4200 mA h g^{-1}) in comparison with that of commercialized graphite (*ca.* 372 mA h g^{-1}).[1,2] The major obstacles to the practical use of Si anodes in lithium-ion batteries are its low intrinsic electric conductivity and the severe volume changes during the Li insertion/extraction process which consequently leads to the pulverization of the active mass particles, and hence permanent capacity fading.[3,4] To overcome these problems, various approaches have been adopted, such as the use of nanosized silicon,[5] surface coating of Si with various conducting materials,[6–9] and Si-based composites.[10–18] Among them, a remarkable strategy is to create Si composites by dispersing nanosize Si particles in a lithium active/inactive matrix. Carbon has been extensively used as an active matrix due to its relatively low mass, good conductivity, small volume change, and reasonable Li-insertion capacity.[15–18]

Recently, conducting polymers, such as polypyrrole[19,20] and polyaniline,[21] have been used as host matrices to make nano-Si composites by utilizing their electrical conductivities and intrinsic flexibilities. These composites showed improved cyclability and rate performance. Conducting polymers can also be used as a carbon source to prepare carbon materials. Wang *et al.* prepared nitrogen doped carbon nanospheres by carbonizing polypyrrole nanospheres which exhibited a reversible capacity of 400 mA h g^{-1} (exceeding the theoretical capacity of graphitic carbon, partly due to the N atom doping effect).[22] Carbonization of heteroatom-containing organic precursors has been widely applied in preparing heteroatom (such as nitrogen, sulfur, and phosphorous) doped carbon materials with improved electrochemical properties.[23–26] With the interest of using conducting polymers as carbon sources, we found that microporous S-doped carbon using a thienyl-based conducting polymer network as the carbon precursor was reported most recently;[27] only polyparaphenylene among the conducting polymers has been used as a carbon source to prepare Si/C composites for the application of lithium-ion battery anode.[28]

Poly(3,4-ethylenedioxythiophene), one of the most successful conducting polymers, has gained great attention for applications in material sciences, in view of its high electrical conductivity in the p-doped state, good thermal and chemical stability, and fast electrochemical switching. Poly(styrenesulfonate) is usually used as a charge-balancing dopant and dispersing agent during polymerization to yield a PEDOT:PSS aqueous suspension. PEDOT:PSS has a high conductivity (*ca.* 10 S cm^{-1}), and good thermal stability with no change in conductivity after treating in air at 100 °C for 1000 h.[29] To date, PEDOT/PEDOT:PSS have been primarily used as cathode materials,[30] or incorporated with other cathode materials, such as $Li_{1.03}Mn_{1.97}O_4$,[31] $LiCoO_2$,[32] and MoS_2,[33] for application in lithium-ion batteries. Additionally, both PEDOT and PSS contain one sulfur atom per repeat unit. It is envisaged that the heteroatom sulfur in amorphous carbon

[a]*Guangzhou Institute of Energy Conversion, Chinese Academy of Sciences, No.2 Nengyuan Rd, Guangzhou, 510640, Guangdong, China. E-mail: lzzhang@ms.giec.ac.cn; Fax: +86 20 37246026; Tel: +86 20 37246025*
[b]*Graduate School of Chinese Academy of Sciences, Beijing, 100039, China*

after carbonizing PEDOT:PSS may improve the electrochemical performance when serving as anode materials.[23,24] Therefore, it is of interest to prepare Si/PEDOT:PSS and the Si/C composite using PEDOT:PSS as a conducting polymer matrix and carbon source for lithium-ion batteries, aiming to improve the electronic conductivity and suppress the large Si volume change on cycling.

In this work, we report a novel nano-Si/PEDOT:PSS composite which was prepared by chemically polymerizing 3,4-ethylenedioxythiophene in a PSS water solution containing dispersed nanosize Si particles. The Si/C composite was subsequently obtained by subjecting Si/PEDOT:PSS to carbonization in an inert atmosphere, whereas the sulfur doping state in the carbon matrix of the Si/C composite was characterized by EDS and XPS. The structural characterizations and electrochemical properties of these composites have been investigated in detail.

2. Results and discussion

Structural characterization

FTIR spectroscopy was used to characterize the formation of the Si/PEDOT:PSS composite and the carbonization of the PEDOT:PSS matrix in Si/C composite. Fig. 1 presents the FTIR spectra of Si/PEDOT:PSS and Si/C composites, along with that of EDOT, PSS and nano-Si particles for comparison. The characteristic peak of EDOT, the =C–H deformation vibration at 891 cm^{-1}, disappeared in the Si/PEDOT:PSS sample. Furthermore, the –C–S– bond at 980 cm^{-1}, the stretching vibration of the –C–O–C– bond at 1090 cm^{-1}, and the C–C and C=C stretches of the quinoidal structure originating from the thiophene ring at 1338 cm^{-1}, were clearly observed in the spectrum of Si/PEDOT:PSS.[25,34] All these typical bands indicate the successful polymerization of EDOT and the formation of the Si/PEDOT:PSS composite. To prepare the Si/C composite, Si/PEDOT:PSS was subjected for carbonization at 800 °C for 3 h under an Ar atmosphere. The typical bands of the thiophene ring at 1338 cm^{-1} from PEDOT and the benzene ring at 1448 cm^{-1} from PSS disappeared after carbonization, indicating that PEDOT:PSS was transformed into carbon.

TGA was carried out to estimate the Si content in the Si/PEDOT:PSS and Si/C composites. Under an air atmosphere, the Si powder sample has an increased weight of 0.78 wt% due to the partial oxidation of Si particles; PEDOT:PSS has a burned residue of 7.26 wt%; Si/PEDOT:PSS has a final retained weight of 59.0 wt% (Fig. 2). Therefore, the Si content in the Si/PEDOT:PSS composite can be calculated to be 51.0 wt% by subtracting the increased weight of Si and the retained weight of PEDOT:PSS from the retained weight of Si/PEDOT:PSS. In order to estimate the Si content in the Si/C composite, the Si/PEDOT:PSS sample was heated following the exact carbonization procedure for preparing the Si/C composite; heating to 800 °C at a rate of 3 °C min^{-1} under an Ar atmosphere and keeping it at 800 °C for 3 h. It was found that the sample retained a weight of 65.9 wt% while heating to 800 °C, and continued losing some of its weight at 800 °C for 3 h with an eventual retained weight of 60.2 wt% (Si/PEDOT:PSS (Ar), Fig. 2) which is very close to the value of 59.0 wt% for the air-heated sample. The Si content in the Si/C composite was then calculated to be 84.7 wt% by dividing the Si content (51.0 wt%) in Si/PEDOT:PSS by the final weight (60.2 wt%) for the Ar-heated Si/PEDOT:PSS sample.

XRD measurements were conducted to examine the structure of the Si composites (Fig. 3). The nano-Si powder sample pattern displays typical diffraction peaks at 2θ of about 28.4°, 47.4°, 56.2°, 69.2° and 76.5° (Fig. 3a), corresponding to the (111), (220), (311), (400) and (331) planes of Si crystals, respectively.[35] The Si/PEDOT:PSS sample shows a diffraction peak at 26.0°, corresponding to the (020) crystalline plane of PEDOT (Fig. 3b inset).[36]

For the Si/C composite, no diffraction lines of crystalline carbon (graphite) were observed. Instead, a broad and weak diffraction peak was observed between 20.0° and 25.0° (Fig. 3c inset), indicating an amorphous nature of the carbon in the composite.[37]

SEM and TEM images of nano-Si particles show that the particle size ranges from 30 to 50 nm with a spherical shape (Fig. 4a/b). The Si/PEDOT:PSS composite consists of large agglomerates with nano-Si particles embedded in a shapeless PEDOT:PSS matrix (Fig. 4c/d). This morphology characteristic was also found in the Si/polypyrrole composite.[20] SEM images of the Si/C composite show similar morphological features: the Si/C

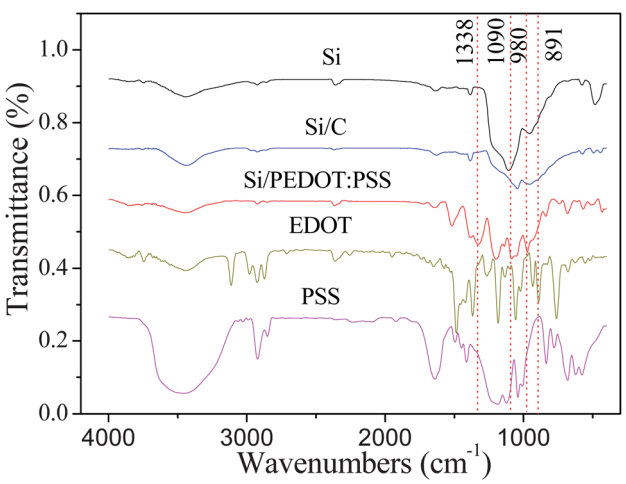

Fig. 1 FTIR spectra of nano-Si, Si/PEDOT:PSS, Si/C, EDOT and PSS.

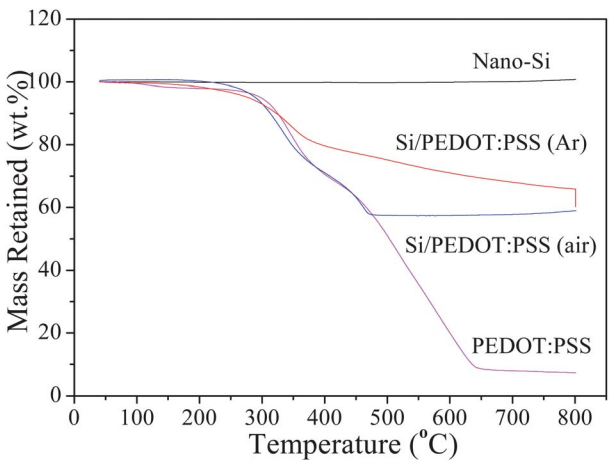

Fig. 2 TGA curves of the bare nano-Si, PEDOT:PSS, and Si/PEDOT:PSS composites under Ar/air atmospheres.

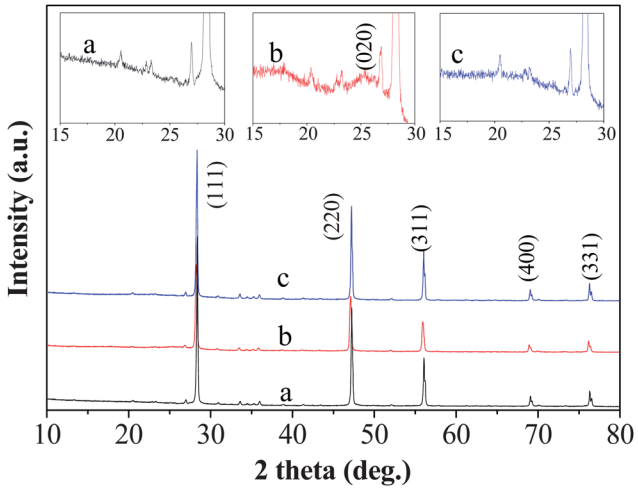

Fig. 3 XRD patterns of nano-Si (a), Si/PEDOT:PSS (b), and Si/C (c).

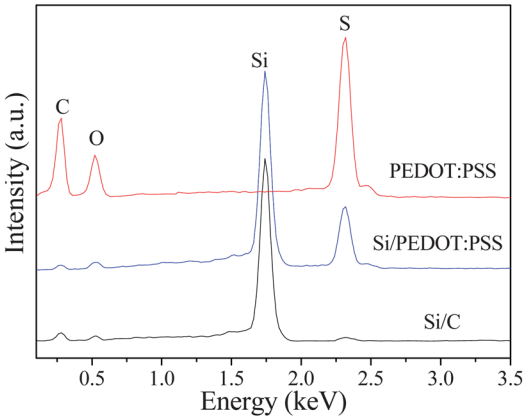

Fig. 5 EDS spectra from nano-Si, PEDOT:PSS, Si/PEDOT:PSS and Si/C.

agglomerates with nano-Si particles enveloped separately and completely in a shapeless carbon matrix (Fig. 4e/f). EDS analysis showed that four different elements, C, O, Si and S, exist both for the Si/PEDOT:PSS and Si/C composites (Fig. 5). The weight ratio of S in the Si/PEDOT:PSS and Si/C composites was 20.6 wt% and 1.14 wt%, respectively. For Si/C, 2.66 wt% of the S element related to the carbon weight was doped in amorphous carbon after carbonizing Si/PEDOT:PSS. The oxygen element in these composites can be ascribed to the contribution from PEDOT:PSS, and/or partially from the oxidation layer of nano-Si particles. XPS experiments were carried out to further investigate the bonding state of the S atom in the Si/PEDOT:PSS and Si/C composite (Fig. 6). The XPS spectrum S(2p) for the Si/PEDOT:PSS composite appears in two components, one at low binding energies with two peaks at 164.0 and 165.2 eV and another at higher binding energies with four peaks at 168.0, 168.4, 169.2 and 169.6 eV contributed by PEDOT and PSS, respectively.[38] The XPS spectrum S(2p) for the Si/C composite has two peaks at 162.7 and 168.1 eV, corresponding to the state of S^{2-} (–C–S–C–) and S^{4+} (–C–SO_3–C–), respectively.[24,39] The –C–S–C– form of the doped sulfur in the amorphous carbon anode can increase the charge capacity of the cells,[23,24] which may have a favorable effect on improving the electrochemical performance of our Si/C composite.

Electrochemical characterization

Fig. 7 displays the charge–discharge voltage profiles of the Si, Si/PEDOT:PSS and Si/C electrodes. It was found that all profiles show the typical charge–discharge plateau of Si at about 0.4 V/0.2 V (*vs.* Li/Li^+), respectively. The bare nano-Si electrode showed a relatively high initial charge–discharge capacity of 1710/1982 mA h g^{-1}, respectively (Fig. 7a). The capacity then degraded quickly due to the cracking and pulverization of the Si electrode over cycling as expected.[40] The Si/PEDOT:PSS anode showed a lower initial charge–discharge capacity (936/1096 mA h g^{-1}), but a higher initial coloumbic efficiency (85.4%) compared with that (73.1%) of the nano-Si anode. After 20 cycles, it can still obtain a discharge capacity of 664 mA h g^{-1}. Unluckily, the capacity decreased to 257 mA h g^{-1} at the 50th cycle (Fig. 7b).

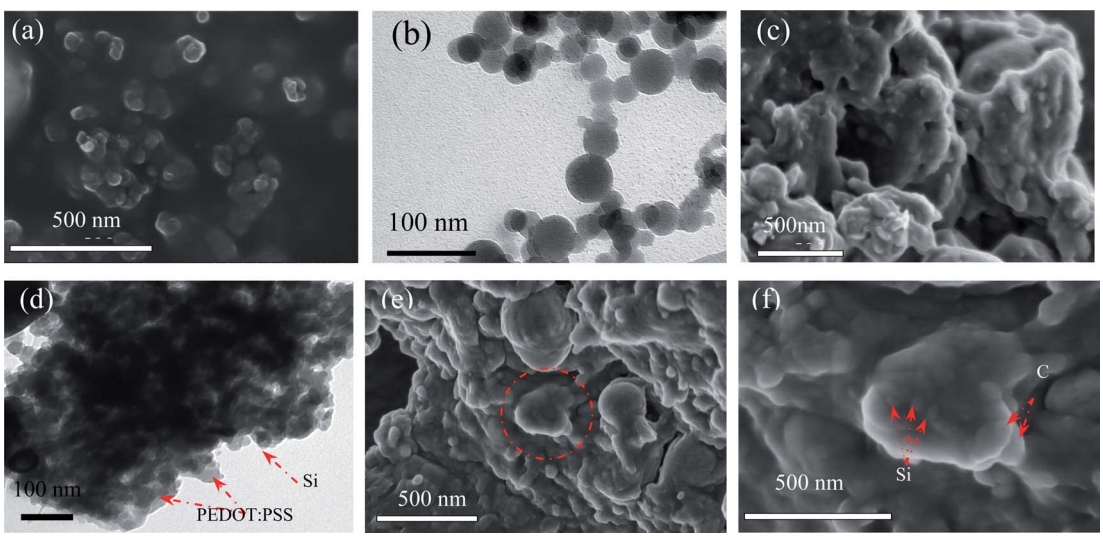

Fig. 4 (a) SEM image and (b) TEM image of nano-Si, (c) SEM image and (d) TEM image of Si/PEDOT:PSS, (e, f) SEM images of Si/C.

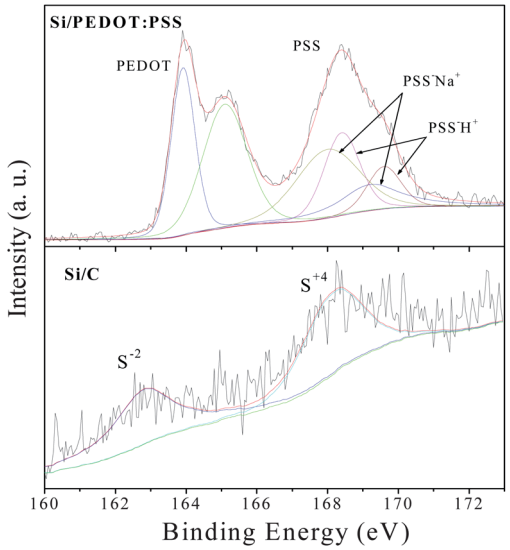

Fig. 6 XPS spectra of S(2p) for the Si/PEDOT:PSS and Si/C composites.

The Si/C composite electrode exhibited both high initial charge–discharge capacities of 1215/1250 mA h g^{-1}, respectively (Fig. 7c). It is worth noting that the Si/C composite has an initial irreversible capacity loss of 2.8% which is far lower than that of nano-Si (26.9%) and Si/PEDOT:PSS (14.6%). The cycling performance of nano-Si, Si/PEDOT:PSS and Si/C at a current density of 100 mA g^{-1} is displayed in Fig. 8. The Si/PEDOT:PSS electrode showed an improved cycling performance compared with the nano-Si electrode without polymer coating, especially for the first 60 cycles. This demonstrates that PEDOT:PSS, as an elastic conducting matrix, efficiently prevented the initial fast capacity loss usually observed in Si based electrodes.[33] Then the capacity of Si/PEDOT:PSS declined to a comparable level with the nano-Si electrode, which is similar to that reported for the nano-Si/polypyrrole system.[41] After 80 cycles, the reversible capacities for the nano-Si, Si/PEDOT:PSS and Si/C composites were 128, 172 and 768 mA h g^{-1}, respectively. The Si/C composite electrode exhibited the best cycling stability with a small capacity fading rate of 0.48% per cycle over 80 cycles. The great retention can be only attributed to the confinements of the S-doped carbon matrix surrounding the nano-Si particles which suppressed the severe volume changes of Si particles over cycling.

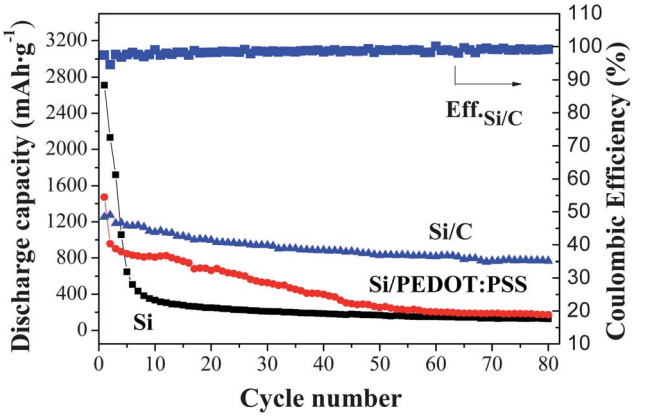

Fig. 8 Cycling performance of nano-Si, Si/PEDOT:PSS, the Si/C composite; and the coloumbic efficiency of the Si/C composite.

Fig. 9 compares the Nyquist plots of bare nano-Si, Si/PEDOT:PSS and the Si/C electrode. All the Nyquist plots include a semicircle and a linear part, indicating that the electrode reactions are controlled by a mixture of charge transfer and diffusion steps.[42] The semicircle part at high frequencies reflects the charge transfer process and the sloping straight line at low frequencies corresponds to the Li-ion diffusion in the bulk

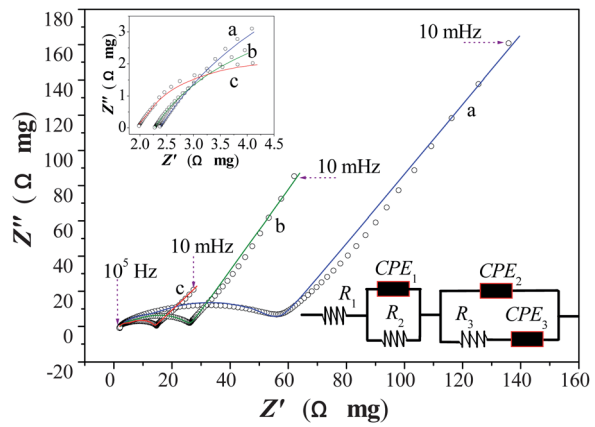

Fig. 9 Nyquist plots of Si (a), Si/PEDOT:PSS (b) and Si/C (c) electrodes at an open circuit potential of 0.45 V. The spots correspond to the experimental data, the solid lines stand for the calculated data from the equivalent circuits (inset).

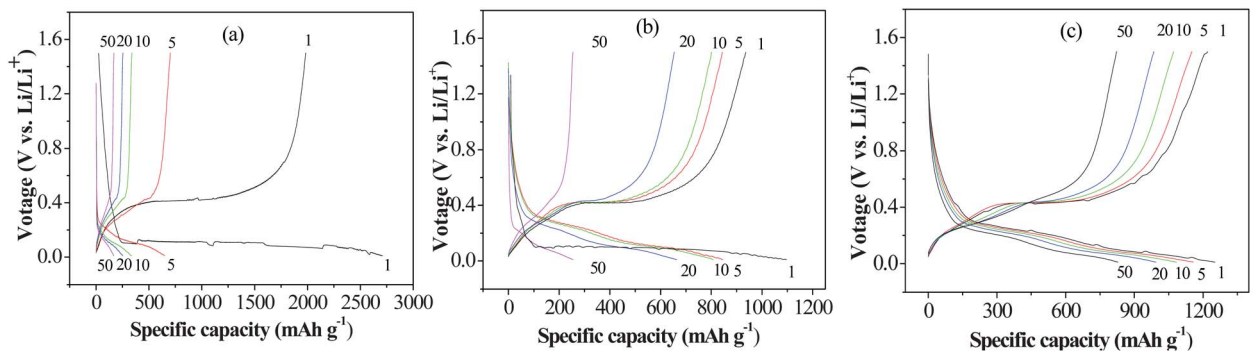

Fig. 7 The charge–discharge curves of nano-Si (a), Si/PEDOT:PSS (b) and Si/C (c).

Table 1 Fitting parameters for the Nyquist plots in Fig. 9

Samples	R_1(Ω·mg)	R_2(Ω·mg)	CPE_1		R_3 (Ω·mg)	CPE_2		CPE_3	
			$Y_{0,1}$ (μF)	n_1		$Y_{0,2}$ (μF)	n_2	$Y_{0,3}$ (μF)	n_3
Si	2.37	7.46	3.71	0.85	47.17	12.15	0.65	3.04	0.70
Si/PEDOT:PSS	2.27	3.62	10.33	0.84	20.43	25.23	0.69	9.09	0.74
Si/C	1.98	2.26	10.98	1.00	9.35	52.01	0.80	11.25	0.64

electrode.[43] Nyquist plots were fitted with the equivalent circuit shown in Fig. 9 (inset). In the equivalent circuit, R_1 is composed of electrolyte resistance (R_s) and electrode resistance (R_e); R_2 represents the passive film resistance which is proportional to the thickness of SEI film; R_3 represents the charge–transfer resistance across the electrode–electrolyte interface; CPE_1 is the constant-phase element which represents the diffusion capacitance attributed to Li-ion diffusion in the solid electrolyte interface (SEI) film; CPE_2 is the electric double-layer capacitance of electrode–solution interface while CPE_3 represents the diffusion capacitance attributed by the diffusion process of the Li-ion in the pore channel of the electrode materials.[44]

Table 1 lists the parameters obtained from fitting the impedance plots. Si/PEDOT:PSS and Si/C composites have a smaller R_1, which means that the electronic conductivity was improved when the nano-Si powders were modified with conductive PEDOT:PSS and carbon. R_2 values are smaller for Si composites, which usually favors the fast transport of Li^+ ions.[45] We can also see that the values of $Y_{0,1}$, $Y_{0,2}$ and $Y_{0,3}$ for Si-composites are higher than that of the nano-Si electrode. The increase of $Y_{0,2}$ which represents the electric double-layer capacitance favors the charge transfer for the electrode reaction. And the increase of $Y_{0,1}$ and $Y_{0,3}$ favors the diffusion of the Li-ion in the SEI film and within the pore channels in the electrode, respectively. Furthermore, R_3 of the Si/PEDOT:PSS and Si/C electrodes, corresponding to the charge-transfer resistance in the electrode–electrolyte interface, is about half and one-fifth of that for nano-Si electrode, respectively. Based on EIS analysis, Si/C composite exhibited the best electrochemical characteristics, the lowest resistances and highest capacitances (Table 1), enabling the Si/C electrode with reduced polarization while cycling; and thus a better cycling performance.

Conclusions

Nanosize Si/PEDOT:PSS and Si/C composites were synthesized by an *in situ* polymerization of EDOT in PSS water solution with dispersed nanosize Si particles and subsequent carbonization of Si/PEDOT:PSS. SEM, TEM, and XRD experiments showed that nanosized Si particles are dispersed homogeneously in PEDOT:PSS and in the amorphous carbon matrix in the Si/PEDOT:PSS and Si/C composites. EDS and XPS results revealed that 2.66 wt% sulfur was doped in the carbon matrix of the Si/C composite. Both of the composites showed higher initial coloumbic efficiencies and better cycling performances than the bare nano-Si when used as electrodes in a lithium-ion half cell. The Si/C composite exhibited the best electrochemical performance, retaining a specific capacity of 768 mA h g^{-1} and a Coloumbic efficiency of 99.2% after 80 cycles, with a very small initial capacity loss of 2.8% and a capacity fade of 0.48% per cycle.

Experimental

Materials and equipment

EDOT (99%) was purchased from Sigma-Aldrich Co. and used without further purification. $Fe_2(SO_4)_3$ (>99%) and $(NH_4)S_2O_8$ (>98%) were purchased from Tianjin Fuchen Chemicals Reagent Factory (China). PSS (average M_W: 70, 000) was obtained from Acros Organics (USA). Nanosize Si powder with average particle sizes of 30–50 nm was purchased from Xuzhou Jiechuang New Material Technology Co. (China). The electrolyte of 1 M $LiPF_6$ in ethylene carbonate (EC, ≥99.9%)/diethylene carbonate (DEC, ≥99.9%) (v/v = 1/1, water content <10 ppm) was purchased from Zhangjiagang Guotai-Huarong New Chemical Materials Co. (China). Other reagents used in this work were purchased from Sinopharm Group Pharmaceutical Co. Ltd. (China) and used as received.

Fourier transform infrared spectroscopy (FTIR) was recorded on a TENSOR 27 spectrometer (Bruker, Germany) from 4000 to 400 cm^{-1} at a resolution of 4 cm^{-1}. Thermal gravimetric analysis (TGA) measurements were conducted on a STA409C/PC-PFEIFFER VACUUMTGA-7 analyzer (NETZSCH-Gertebau GmbH, Germany) in either air or an Ar atmosphere with a flow rate of 30 mL min^{-1} from 40 °C to 800 °C at a heating rate of 3 °C min^{-1}. The morphologies of the Si composites were observed by a scanning electron microscope (SEM; Hitachi S-4800, Japan) with an energy dispersive spectroscopy (EDS) detector and transmission electron microscope (TEM; FEI-Tecnai 12, Netherlands). The XPS spectra were obtained with ESCALAB250 XPS (Thermo Fisher Scientific, USA) at 2×10^{-9} mba. Al Kα (1486.6 eV) was used as the X-ray source at 15 keV of anode voltage. The filament current and emission current were 4.6 A and 20 mA, respectively. The phase identification was performed by X-ray diffraction (XRD, PANALYTICAL Incorporated, Netherlands) from 10° to 80°. Electrochemical impedance spectroscopy (EIS) results were obtained with a Zennium/IM6 electrochemical workstation (Zahner, Germany).

Synthesis of Si composites

The Si/PEDOT:PSS composite was prepared by dispersing nano-Si particles in an aqueous solution of EDOT and PSS, followed by a chemical polymerization of EDOT using $(NH_4)S_2O_8$/$Fe_2(SO_4)_3$ as a catalyst.[46] A typical procedure is described as follows. EDOT (0.28 g) was added to a solution of PSS (0.82 g) in 90 mL deionized water, and stirred further for 1 h. In this solution, Si particles (0.40 g) were added and dispersed under

vigorous stirring. The pH value of the solution mixture was adjusted to 2 by adding 2 M HCl solution. The catalyst solution of $(NH_4)S_2O_8$ (0.70 g)/$Fe_2(SO_4)_3$ (6 mg) in 10 mL water was then added to the reaction mixture in an ice/water bath. After stirring for 24 h, the Si/PEDOT:PSS composite was obtained as a dark blue powder, after filtration, washing 3 times with DI water and once with absolute ethanol, and drying under vacuum at 60 °C for 24 h. The Si/C composite was prepared by subjecting the as-prepared Si/PEDOT:PSS composite for carbonization at 800 °C for 3 h under an Ar atmosphere at a heating rate of 3 °C min^{-1}.

Characterization of electrochemical properties

The coin cells (CR2025) were assembled to test the electrochemical performance of the prepared nano-Si composites and bare nano-Si powder for comparison. The Si/PEDOT:PSS composite, Si/C and bare nano-Si powder electrode was prepared by mixing with acetylene black and carboxymethyl cellulose, at a weight ratio of 62 : 30 : 8 in an aqueous solution to form a homogeneous slurry. The slurry was spread onto a copper foil. The obtained electrodes were then dried at 60 °C in a vacuum oven for 12 h and pressed to enhance the contact between the active materials and conductive carbon. The half cells were assembled in an Ar filled glove-box, using 1 M $LiPF_6$ EC/DEC (v/v = 1/1) as the electrolyte and Li foil as the counter electrode. The cells were then galvanostatically charged and discharged at a constant current density of 100 mA g^{-1} in a voltage range of 0.01–1.5 V (*vs.* Li/Li^+). The capacity of the composites was calculated based on the whole composite as active mass.

EIS was measured by applying an alternating voltage of 5 mV over the frequency ranging from 10^{-2} to 10^5 Hz. All impedance measurements were carried out at a first discharged potential of 0.45 V (*vs.* Li/Li^+) at 25 °C.

Acknowledgements

This work was supported by the National Science Foundation of China (50973112), the Hundred Talents Program of the Chinese Academy of Sciences (CAS), CAS-Guangdong Collaboration Program (2009B091300025), and Science & Technology Project of Guangzhou (China).

Notes and References

1 M. Winter, J. O. Besenhard, M. Spahr and P. Novak, *Adv. Mater.*, 1998, **10**, 725.
2 S. Hossain, Y. K. Kim, Y. Saleh and R. Loutfy, *J. Power Sources*, 2003, **114**, 264.
3 B. C. Kim, H. Uono, T. Satou, T. Fuse, T. Ishihara, M. Ue and M. Senna, *J. Electrochem. Soc.*, 2005, **152**, A523.
4 C. K. Chan, R. Ruffo, S. S. Hong, R. A. Huggins and Y. Cui, *J. Power Sources*, 2009, **189**, 34.
5 J. R. Szczech and S. Jin, *Energy Environ. Sci.*, 2011, **4**, 56; and references therein.
6 J. W. Kim, J. H. Ryu, K. T. Lee and S. M. Oh, *J. Power Sources*, 2005, **147**, 227.
7 M. Yoshio, H. Wang, K. Fukuda, T. Umeno, N. Dimov and Z. Ogumi, *J. Electrochem. Soc.*, 2002, **149**, A1598.
8 W. R. Liu, J. H. Wang, H. C. Wu, D. T. Shieh, M. H. Yang and N. L. Wu, *J. Electrochem. Soc.*, 2005, **152**, A1719.
9 H. X. Chen, Y. Xiao, L. Wang and Y. Yang, *J. Power Sources*, 2011, **196**, 6657.
10 T. Hasegawa, S. R. Mukai, Y. Shirota and T. Tamon, *Carbon*, 2004, **42**, 2573.
11 J. Y. Eom, J. W. Park, H. S. Kwon and S. Rajendran, *J. Electrochem. Soc.*, 2006, **153**, A1678.
12 J. Shu, H. Li, R. Yang, Y. Shi and X. Huang, *Electrochem. Commun.*, 2006, **8**, 51.
13 W. Wang, M. K. Datta and P. N. Kumta, *J. Mater. Chem.*, 2007, **17**, 3229.
14 U. Kasavajjula, C. S. Wang and A. J. Appleby, *J. Power Sources*, 2007, **163**, 1003.
15 S. H. Ng, J. Z. Wang, D. Wexler, K. Konstantinov, Z. P. Guo and H. K. Liu, *Angew. Chem., Int. Ed.*, 2006, **45**, 6896.
16 H. Kim and J. Cho, *Nano Lett.*, 2008, **8**, 3688.
17 R. Teki, M. K. Datta, R. Krishnan, T. C. Parker, T. M. Lu, P. N. Kumta and N. Koratkar, *Small*, 2009, **5**, 2236.
18 N. Dimov, Y. Xia and M. Yoshio, *J. Power Sources*, 2007, **171**, 886.
19 Z. P. Guo, J. Z. Wang, H. K. Liu and S. X. Dou, *J. Power Sources*, 2005, **146**, 448.
20 S. Y. Chew, Z. P. Guo, J. Z. Wang, J. Chen, P. Munroe, S. H. Ng, L. Zhao and H. K. Liu, *Electrochem. Commun.*, 2007, **9**, 941.
21 J. J. Cai, P. J. Zuo, X. Q. Cheng, Y. H. Xu and G. P. Yin, *Electrochem. Commun.*, 2010, **12**, 1572.
22 Y. Wang, F. B. Su, C. D. Wood, J. Y. Lee and X. S. Zhao, *Ind. Eng. Chem. Res.*, 2008, **47**, 2294.
23 S. Ito, T. Murata, M. Hasegawa, Y. Bito and Y. Toyoguchi, *J. Power Sources*, 1997, **68**, 245.
24 Y. P. Wu, S. B. Fang, Y. Y. Jiang and R. Holze, *J. Power Sources*, 2002, **108**, 245.
25 G. Hasegawa, M. Aoki, K. Kanamori, K. Nakanishi, T. Hanadaa and K. Tadanaga, *J. Mater. Chem.*, 2011, **21**, 2060.
26 J. P. Paraknowitsh, A. Thomas and J. Schmidt, *Chem. Commun.*, 2011, **47**, 8283.
27 Y. P. Wu, S. B. Fang and Y. Y. Jiang, *J. Mater. Chem.*, 1998, **8**, 2223.
28 X. W. Zhang, P. K. Patil, C. S. Wang, A. J. Appleby, F. E. Little and D. L. Cocke, *J. Power Sources*, 2004, **125**, 206.
29 B. L. Groenendaal, F. Jonas, D. Freitag, H. Pielartzik and J. R. Reynolds, *Adv. Mater.*, 2000, **12**, 481.
30 L. Z. Zhan, Z. P. Song, J. Y. Zhang, J. Tang, H. Zhan, Y. H. Zhou and C. M. Zhan, *Electrochim. Acta*, 2008, **53**, 8319.
31 C. Arbizzani, M. Mastragostino and M. Rossi, *Electrochem. Commun.*, 2002, **4**, 545.
32 L. J. Her, J. L. Hong and C. C. Chang, *J. Power Sources*, 2006, **157**, 457.
33 A. V. Murugan, M. Quintin, M. H. Delville, G. Campet, C. S. Gopinath and K. Vijayamohanan, *J. Power Sources*, 2006, **156**, 615.
34 M. Salsamendi, R. Marcilla, M. Dobbelin, D. Mecerreyes, C. Pozo-Gonzalo, J. A. Pomposo and R. Pacios, *Phys. Status Solidi A*, 2008, **205**, 1451.
35 S. H. Ng, J. Wang, D. Wexler, S. Y. Chew and H. K. Liu, *J. Phys. Chem. C*, 2007, **111**, 11131.
36 X. R. Zhong, G. X. Fei and H. S. Xia, *J. Appl. Polym. Sci.*, 2010, **118**, 2146.
37 L. W. Ji and X. W. Zhang, *Carbon*, 2009, **47**, 3219.
38 E. Vitoratos, S. Sakkopoulos, E. Dalas, N. Paliatsas, D. Karageorgopoulos, F. Petraki, S. Kennou and S. A. Choulis, *Org. Electron.*, 2009, **10**, 61.
39 G. Greczynski, Th. Kugler, M. Keil, W. Osikowicz, M. Fahlman and W. R. Salanack, *J. Electron Spectrosc. Relat. Phenom.*, 2001, **121**, 1.
40 S. H. Ng, J. Z. Wang, D. Wexler, K. Konstantinov, Z. P. Guo and H. K. Liu, *Angew. Chem., Int. Ed.*, 2006, **45**, 6896.
41 H. S. La, K. S. Park, K. S. Nahm, K. K. Jeong and Y. S. Lee, *Colloids Surf., A*, 2006, **272**, 22.
42 Z. Y. Zeng, J. P. Tu, X. L. Wang and X. B. Zhao, *J. Electroanal. Chem.*, 2008, **616**, 7.
43 J. Y. Song, H. H. Lee, Y. Y. Wang and C. C. Wan, *J. Power Sources*, 2002, **111**, 255.
44 P. J. Zuo, G. P. Yin, J. Zhao, Y. L. Ma, X. Q. Cheng, P. F. Shi and T. Takamura, *Electrochim. Acta*, 2006, **52**, 1527.
45 D. C. Sun and D. S. Sun, *Mater. Chem. Phys.*, 2009, **118**, 288.
46 F. Louwet, L. Groenendaal, J. Dhaen, J. Manca, J. Van Luppen, E. Verdonck and L. Leenders, *Synth. Met.*, 2003, **135**, 115.